

# Small-molecule inhibition of siderophore biosynthesis in *Mycobacterium tuberculosis* and *Yersinia pestis*

Julian A Ferreras<sup>1</sup>, Jae-Sang Ryu<sup>2</sup>, Federico Di Lello<sup>1</sup>, Derek S Tan<sup>2,3</sup> & Luis E N Quadri<sup>1</sup>

***Mycobacterium tuberculosis* and *Yersinia pestis*, the causative agents of tuberculosis and plague, respectively, are pathogens with serious ongoing impact on global public health<sup>1,2</sup> and potential use as agents of bioterrorism<sup>3</sup>. Both pathogens have iron acquisition systems based on siderophores, secreted iron-chelating compounds with extremely high Fe<sup>3+</sup> affinity<sup>4,5</sup>. Several lines of evidence suggest that siderophores have a critical role in bacterial iron acquisition inside the human host<sup>6–9</sup>, where the free iron concentration is well below that required for bacterial growth and virulence<sup>10</sup>. Thus, siderophore biosynthesis is an attractive target in the development of new antibiotics to treat tuberculosis and plague<sup>2,5,8,11</sup>. In particular, such drugs, alone or as part of combination therapies, could provide a valuable new line of defense against intractable multiple-drug-resistant infections. Here, we report the design, synthesis and biological evaluation of a mechanism-based inhibitor of domain salicylation enzymes required for siderophore biosynthesis in *M. tuberculosis* and *Y. pestis*. This new antibiotic inhibits siderophore biosynthesis and growth of *M. tuberculosis* and *Y. pestis* under iron-limiting conditions.**

The two siderophore variants produced by *M. tuberculosis*, the cell-associated and soluble mycobactins (MBTs)<sup>5</sup>, and the *Y. pestis* siderophore, yersiniabactin (YBT)<sup>4</sup>, all have salicyl-capped non-ribosomal peptide-polyketide hybrid scaffolds (Fig. 1a). Although non-ribosomal peptide and polyketide biosynthetic pathways have primarily been studied in the context of engineering biosyntheses of novel 'unnatural products', they may also be viable targets for developing drugs that block the biosynthesis of microbial compounds required for virulence.

Siderophore biosynthesis pathways have undergone extensive investigations<sup>12,13</sup>. The resulting mechanistic understanding of these pathways provides opportunities to design small-molecule inhibitors that block siderophore biosynthesis and, hence, bacterial growth and virulence in iron-limiting environments. These inhibitors would also be powerful chemical genetic tools for deciphering the relevance of siderophores at specific stages of infection because they could be used to provide temporal control of siderophore production in animal models of bacterial infection. During the biosyntheses of MBTs and YBT, domain salicylation enzymes—MbtA and YbtE, respectively—catalyze the salicylation of an aroyl carrier protein

(ArCP) domain to form a salicyl–ArCP domain thioester intermediate through a two-step reaction (Fig. 1b)<sup>14,15</sup>. The first step is ATP-dependent adenylation of salicylate to generate a salicyl-AMP intermediate, 1 (Fig. 1c), which remains bound non-covalently to the active site. The second step is the transesterification of the salicyl moiety onto the thiol of the phosphopantetheinyl prosthetic group of the ArCP domain<sup>14,15</sup>. Because MbtA and YbtE have no homologs in humans, they are particularly attractive targets for the development of antibiotics that inhibit siderophore biosynthesis.

We noted at the outset that other mechanistically related adenylate-forming enzymes have been shown to bind their cognate acyl-AMP intermediates 2–3 orders of magnitude more tightly than their carboxylic acid and ATP substrates<sup>16</sup>. Thus, various non-hydrolyzable acyl-AMP analogs have been used as mechanism-based inhibitors of adenylate-forming enzymes. Among these are the acyl sulfamoyl adenosines (acyl-AMS)<sup>16,17</sup>, inspired by the natural product nucleocidin<sup>18</sup>, 4 (Fig. 1c). Based on these considerations, we postulated that the reaction intermediate mimic 5'-O-(N-salicylsulfamoyl)adenosine (salicyl-AMS), 2, would be a potent inhibitor of the salicylate adenylation activity of MbtA, YbtE, and closely related enzymes such as PchD, the domain salicylation enzyme that is involved in the biosynthesis of the siderophore pyochelin in *Pseudomonas aeruginosa*<sup>19</sup> (Fig. 1a).

To evaluate this idea further, we examined the reported cocrystal structure of a related adenylate-forming enzyme, DhbE, in complex with its cognate 2,3-dihydroxybenzoyl-AMP intermediate<sup>20</sup>, 3 (Fig. 1c). The intermediate is bound by a substantial number of interactions, and we identified the probable key binding residues (Supplementary Fig. 1 online). We then performed full-length amino acid sequence alignments of DhbE, MbtA, YbtE, PchD and three other related aroyl adenylate-forming enzymes. Overall sequence identities were ≈40–50%; however, the putative aroyl-AMP binding residues were almost completely conserved in all of the enzymes, except for minor differences at the base of the binding pocket that are likely to contribute to specificity for salicylate as compared with 2,3-dihydroxybenzoate<sup>20</sup>. This suggested that salicyl-AMP is likely to bind to MbtA, YbtE and PchD in a similar fashion and, because binding of the phosphate group of 2,3-dihydroxybenzoyl-AMP seems to involve primarily hydrogen-bonding interactions rather than electrostatic interactions, we postulated that the uncharged sulfamate group in salicyl-AMS would be a viable surrogate for the phosphate group in salicyl-AMP.

<sup>1</sup>Department of Microbiology and Immunology, Weill Medical College of Cornell University, 1300 York Ave., Box 62, New York, New York 10021, USA. <sup>2</sup>Molecular Pharmacology and Chemistry Program and <sup>3</sup>Tri-Institutional Research Program, Memorial Sloan-Kettering Cancer Center, 1275 York Ave., Box 422, New York, New York 10021, USA. Correspondence should be addressed to L.E.N.Q. (leq2001@med.cornell.edu) or D.S.T. (tand@mskcc.org).

Published online 24 May 2005; doi:10.1038/nchembio706

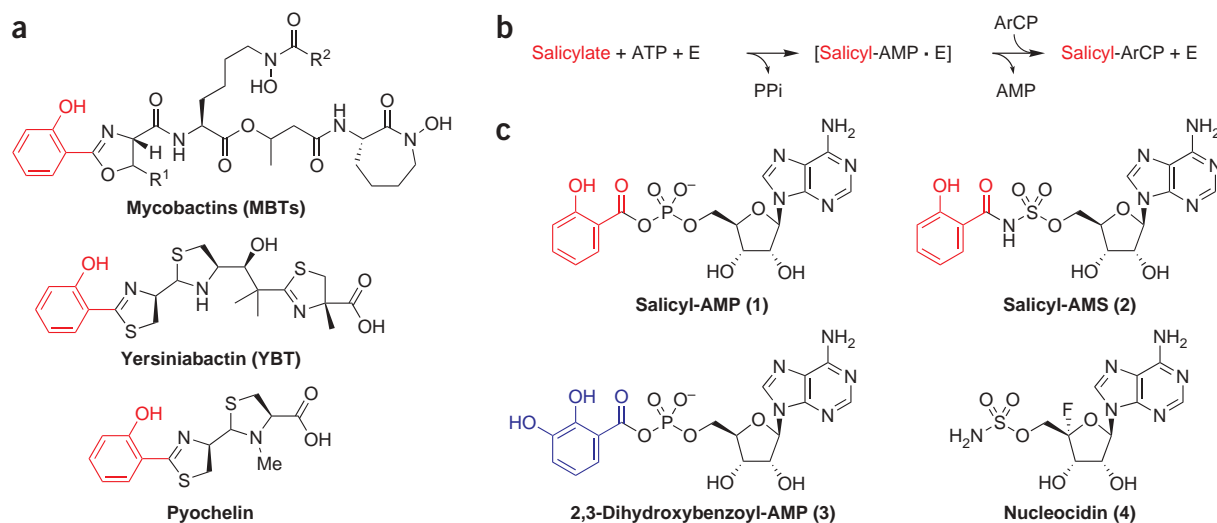


**Figure 1** Structures of salicyl-capped siderophores, aroyl-adenylate biosynthesis intermediates, and intermediate mimics. **(a)** Mycobactins, yersiniabactin and pyochelin. The salicyl moiety is highlighted in red. Cell-associated mycobactins:  $R^1 = H$ ;  $R^2 = (CH_2)_{16-19}CH_3$ ,  $(CH_2)_nCH=CH(CH_2)_mCH_3$ ,  $(n + m) = 14-17$ . Soluble mycobactins:  $R^1 = H, Me$ ;  $R^2 = (CH_2)_{1-7}COOCH_3$ ,  $(CH_2)_{1-7}COOH$ ,  $(CH_2)_nCH=CH(CH_2)_mCOOCH_3$ ,  $(CH_2)_nCH=CH(CH_2)_mCOOH$ ,  $(n + m) = 1-5$ . **(b)** Two-step ArCP-domain salicylation reaction. **(c)** Salicyl-AMP reaction intermediate, **1**; its salicyl-AMP mimic, **2**; the 2,3-dihydroxybenzoyl-AMP reaction intermediate, **3**; and the related antibiotic nucleocidin, **4**.

We therefore synthesized salicyl-AMS (**Supplementary Fig. 2** online) and used an adenylation assay (Methods) to determine dose-response curves for inhibition of the adenylation activity of MbtA, YbtE and PchD at fixed, saturating substrate concentrations. An initial inspection indicated that the  $IC_{50}$  values were similar to the enzyme concentrations (within a factor of 10), a characteristic of tight-binding inhibitors (TBIs)<sup>21</sup>. On the basis of this observation and the large number of binding interactions in the aroyl-AMP binding model discussed earlier, we hypothesized that salicyl-AMS behaves as a TBI. Notably, the steady-state approximations that permit application of the Henri-Michaelis-Menten equation to characterize inhibitor-enzyme interactions are not applicable to TBIs because of their high binding affinity. Instead, methodologies that consider an alternative steady-state approach are more appropriate for analysis of TBIs<sup>21</sup> and were used in our study. With this approach,  $IC_{50}$  values were  $10.7 \pm 2.0$  nM for MbtA (**Fig. 2a**),  $14.7 \pm 2.0$  nM for YbtE (**Fig. 2b**) and  $12.5 \pm 2.2$  nM for PchD (**Fig. 2c**). These values are  $\approx \frac{1}{2} [E]$  and

consistent with the expected 1:1 stoichiometry for the enzyme-inhibitor complexes. In contrast to salicyl-AMS, the parental compound 5'-*O*-sulfamoyladenine (AMS), **8** (**Supplementary Fig. 2**), did not inhibit adenylation when tested at up to 400 nM under the same conditions (data not shown).

We selected YbtE for further analysis of salicyl-AMS and observed a linear relationship between the  $IC_{50}$  values and YbtE concentrations, with a slope of 0.43 ( $R^2 = 0.9594$ ), corrected to 0.52 ( $R^2 = 0.9999$ ) when the YbtE concentrations derived from the dose-response curve fits were used to adjust for errors in enzyme concentration and the inactive protein fraction (**Fig. 2d**). As a slope of 0.5 is diagnostic of a TBI modality<sup>21</sup>, the results support our hypothesis that salicyl-AMS acts as a TBI.

We next determined  $K_i^{app}$  (apparent inhibition constant) values from dose-response curves using variable ATP or salicylate concentrations. The  $K_i^{app}$  values increased linearly with increasing ATP concentration over a range of  $0.2-60 \times K_m^{ATP}$  and excess salicylate

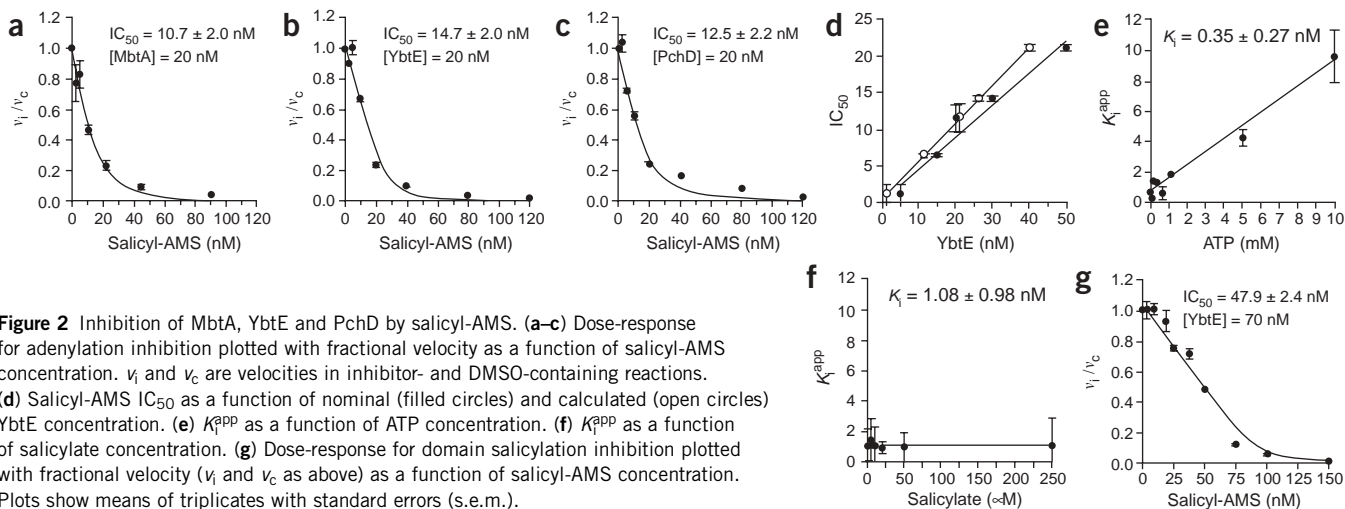


**Figure 2** Inhibition of MbtA, YbtE and PchD by salicyl-AMS. **(a-c)** Dose-response for adenylation inhibition plotted with fractional velocity as a function of salicyl-AMS concentration.  $v_i$  and  $v_c$  are velocities in inhibitor- and DMSO-containing reactions. **(d)** Salicyl-AMS  $IC_{50}$  as a function of nominal YbtE concentration (filled circles) and calculated YbtE concentration (open circles). **(e)**  $K_i^{app}$  as a function of ATP concentration. **(f)**  $K_i^{app}$  as a function of salicylate concentration. **(g)** Dose-response for domain salicylation inhibition plotted with fractional velocity ( $v_i$  and  $v_c$  as above) as a function of salicyl-AMS concentration. Plots show means of triplicates with standard errors (s.e.m.).

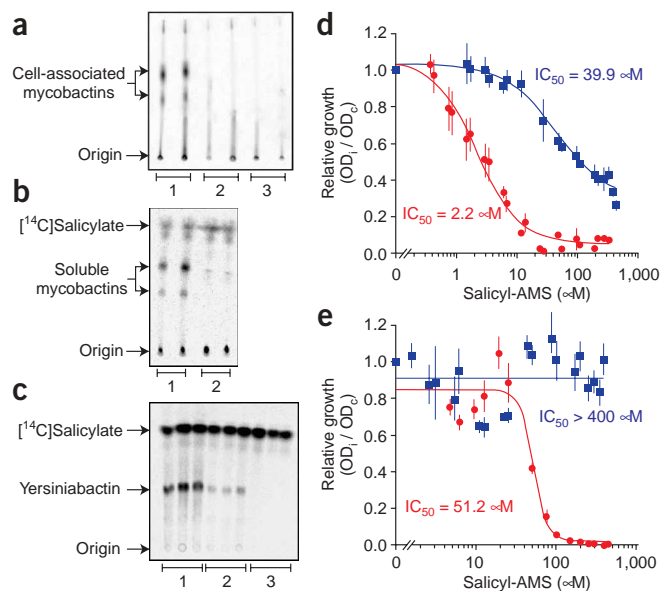


**Figure 3** Inhibition of siderophore production and bacterial growth by salicyl-AMS. (a–c) TLC of cell-associated mycobactins (a), soluble mycobactins (b) and yersiniabactin (c). Lanes 1, 2 and 3 show siderophores extracted from DMSO-treated cultures, inhibitor-treated cultures and siderophore-deficient strains *M. tuberculosis* (a) and *Y. pestis* (c), respectively. Replicate lanes are marked. (d,e) Growth inhibition of *M. tuberculosis* (d) and *Y. pestis* (e) in iron-deficient (filled red circles) or iron-supplemented (filled blue squares) media as a function of salicyl-AMS concentration. OD<sub>i</sub> and OD<sub>c</sub>, optical density of inhibitor- and DMSO-treated cultures. Plots show means of triplicates with s.e.m.

( $\approx 190 \times K_m^{\text{Sal}}$ ) (Fig. 2e). This result is indicative of competitive inhibition with respect to ATP<sup>21</sup>, and thus a  $K_i$  value of  $0.35 \pm 0.27$  nM was calculated as the  $y$  intercept of the line fitted to the data in Figure 2e. In contrast, increasing salicylate concentration from  $0.2$ – $50 \times K_m^{\text{Sal}}$  in the presence of excess ATP ( $\approx 60 \times K_m^{\text{ATP}}$ ) had no appreciable effect on  $K_i^{\text{APP}}$  (Fig. 2f). This is diagnostic of non-competitive inhibition with respect to this substrate<sup>21</sup>, and a  $K_i$  of  $1.08 \pm 0.98$  nM was calculated by averaging the  $K_i^{\text{APP}}$  values. Overall, our data confirmed that salicyl-AMS behaves as a potent inhibitor of YbtE with a tight-binding modality.

Our results above demonstrate that salicyl-AMS inhibits the first step of the ArCP domain salicylation reaction catalyzed by YbtE, MbtA and PchD (Fig. 1b). Thus, the inhibitor should also block formation of the salicyl-ArCP domain intermediate. To investigate this hypothesis, we developed a domain salicylation assay using YbtE, a phosphopantetheinylated His<sub>6</sub>-tagged ArCP domain fragment (ypArCP-H6, 108 residues) from the *Y. pestis* HMWP2 synthetase (a multidomain enzyme involved in YBT synthesis<sup>15</sup>), and 96-well flash plates (Methods). The flash plate wells have a Ni<sup>2+</sup> coat for ypArCP-H6 binding and a scintillant coat that provides a scintillation proximity effect for detection of the YbtE-catalyzed incorporation of [<sup>3</sup>H]salicylate into well-bound ypArCP-H6. In this assay, salicyl-AMS potently inhibited [<sup>3</sup>H]salicyl-ypArCP-H6 formation, with an  $IC_{50} \approx \frac{1}{2}[E]$  (Fig. 2g). In contrast, AMS did not inhibit salicylation when tested at up to 400 μM under the same conditions (data not shown). Thus, the results of this domain salicylation assay are in agreement with those obtained using the salicylate adenylation assay described earlier.

Having demonstrated that salicyl-AMS inhibits MbtA and YbtE, we next examined the ability of this compound to block siderophore biosynthesis in *M. tuberculosis* and *Y. pestis*. Radiometric siderophore production assays (Methods) showed that salicyl-AMS inhibits both MBT production in *M. tuberculosis* and YBT production in *Y. pestis* (Fig. 3a–c). Under the conditions tested, MBT production was virtually undetectable and YBT production was inhibited by approximately fivefold relative to DMSO-treated controls.

Because siderophore biosynthesis is required for efficient bacterial growth under iron-limiting conditions, we assessed the effect of salicyl-AMS on *M. tuberculosis* and *Y. pestis* growth in iron-deficient culture media. Indeed, salicyl-AMS inhibited the growth of both

organisms under these conditions (*M. tuberculosis*:  $IC_{50} = 2.2 \pm 0.3$  μM; *Y. pestis*:  $IC_{50} = 51.2 \pm 4.7$  μM) (Fig. 3d,e). Furthermore, salicyl-AMS (tested at up to  $8 \times IC_{50}$ ) was not active against *Y. pestis* in iron-supplemented medium (Fig. 3e), in which siderophore production is not required for growth. Under these conditions, salicyl-AMS (tested at up to  $180 \times IC_{50}$ ) did inhibit *M. tuberculosis* growth, albeit with an 18-fold increase in  $IC_{50}$  ( $39.9 \pm 7.6$  μM) (Fig. 3d). This suggests that, in addition to blocking siderophore biosynthesis, salicyl-AMS may also inhibit *M. tuberculosis* growth by other mechanisms. Efforts to develop optimized analogs of salicyl-AMS with increased cellular potency and specificity are ongoing in our laboratories.

To our knowledge, salicyl-AMS is the first biochemically confirmed inhibitor of siderophore biosynthesis<sup>5</sup>. Consistent with this activity, salicyl-AMS also inhibits the growth of *M. tuberculosis* and *Y. pestis* under iron-limiting conditions. Thus, salicyl-AMS is a promising initial lead compound for the development of new antibiotics to treat tuberculosis and plague.

## METHODS

**Salicyl-AMS synthesis.** Silylation of adenosine, 5, followed by selective deprotection of 5'-O-TBS group provided 2',3'-bis-O-TBS-adenosine, 6 (ref. 22) (Supplementary Fig. 2). We elected to use silyl protecting groups at the 2' and 3' positions to set the stage for future syntheses of analogs to be carried out either in solution or on solid support using a silyl ether linker. Sulfamoylation of 6 at the 5' position using bis(tributyltin) oxide and sulfamoyl chloride<sup>23</sup> provided sulfamate, 7. Salicylate was preactivated with 1,1'-carbonyldiimidazole, then coupled to the sulfamate nitrogen of 7 (ref. 24). Subsequent deblockage of the TBS protecting groups with tetrabutylammonium fluoride afforded salicyl-AMS, 2. The synthesis was accomplished in five steps and with 31% overall yield. Full experimental procedures and compound characterization data are provided in the Supplementary Methods online. Analytical data for salicyl-AMS, 2, are as follows. TLC:  $R_f = 0.33$  (5:1 ethyl acetate/methanol). <sup>1</sup>H NMR (400 MHz, DMSO-*d*<sub>6</sub>):  $\delta$  8.40 (s, 1H), 8.12 (s, 1H), 7.81 (dd, 1H,  $J = 7.7, 1.4$ ), 7.28–7.24 (m, 3H), 6.75 (d, 1H,  $J = 7.7$ ), 6.74 (t, 1H,  $J = 7.7$ ), 5.92 (d, 1H,  $J = 6.4$ ), 5.49 (d, 1H,  $J = 6.1$ ), 5.35 (d, 1H,  $J = 4.8$ ), 4.62 (dd, 1H,  $J = 6.4, 5.8$ ), 4.25–4.08 (m, 4H). <sup>13</sup>C NMR (125 MHz, DMSO-*d*<sub>6</sub>):  $\delta$  160.7, 156.0, 152.6, 149.6, 139.3, 132.6, 129.9, 119.9, 118.9, 117.5, 116.6, 86.9, 82.5, 73.5, 70.8, 68.1, 48.6. ESI-MS  $m/z$ : (pos) 467 [M+H]<sup>+</sup>, 489 [M+Na]<sup>+</sup>; (neg) 465 [M-H]<sup>-</sup>.

**Adenylation assay, domain salicylation assay and data analysis.** Adenylation was measured with an ATP-[<sup>32</sup>P]pyrophosphate exchange assay as reported<sup>14,15,19</sup>. The domain salicylation assay was performed in 96-well Nickel Chelate Coated FlashPlate PLUS plates (flash plates) (Perkin Elmer). Plate wells have a scintillant coat and a Ni<sup>2+</sup> coat for binding of phosphopantetheinylated His<sub>6</sub>-tagged ArCP domain. YbtE-catalyzed incorporation of the [<sup>3</sup>H]salicyl group into the well-bound domain leads to formation of [<sup>3</sup>H]salicyl-ypArCP-H6, which is quantified using a plate counter. All assays were performed using recombinant proteins. Full experimental details of protein production and purification as well as assay conditions and data analysis are provided in the Supplementary Methods.

**Siderophore production assays.** For analysis of mycobacterial siderophores, *M. tuberculosis* H37Rv cultures (500 μl, initial optical density at 580 nm (OD<sub>580</sub>) = 0.2) were grown for 3 d at 37 °C without shaking in

Chelex-100–deferrated GAST medium<sup>8</sup> (GAST-D) containing [<sup>14</sup>C]salicylate (20 μM, 55 mCi/mmol) for siderophore labeling and inhibitor (200 μM) or DMSO (0.25%) in controls. The MBT-deficient *M. tuberculosis* strain *mbtF*<sup>−</sup> (ref. 25), treated with DMSO as described earlier, was used as an additional control in the experiment. Cells pellets of inhibitor- and DMSO-treated cultures were incubated for 12 h with 300 μl ethanol. After incubation, the debris was removed by centrifugation, one volume of water and FeCl<sub>3</sub> (to 2.2 mM) was added to the ethanol supernatant, and cell-associated MBTs were extracted from the mixture twice with one volume of CHCl<sub>3</sub>. For isolation of soluble MBTs, FeCl<sub>3</sub> (to 0.6 mM) was added to culture supernatants before siderophore extraction as described earlier. Extracts were dried and resuspended in CHCl<sub>3</sub> before radiometric-TLC analysis using Al Sil G/UV plates (Whatman) and 2:3:3 petroleum ether/1-butanol/ethyl acetate as the eluent. Plates were exposed to a phosphorimager screen for 72 h and analyzed with a Storm Phosphorimager (Molecular Dynamics). *R<sub>F</sub>* values of MBTs (0.45 and 0.6) were in agreement with those reported<sup>26</sup>. YBT was isolated from supernatants of *Y. pestis* cultures (avirulent strain KIM6-2082.1+ (ref. 27), 200 μl, initial OD<sub>620</sub> = 0.1) grown for 15 h with agitation (220 r.p.m.) at 37 °C in Chelex-100–deferrated PMH medium<sup>6</sup> (PMH-D) containing [<sup>14</sup>C]salicylate for siderophore labeling and inhibitor or DMSO as described earlier. The YBT-deficient *Y. pestis* strain KIM6 2082.1 (ref. 27) treated with DMSO was used as an additional control. Culture supernatants were extracted twice with one volume of ethyl acetate, the organic solvent was evaporated, and the YBT was resuspended in methanol for radiometric-TLC analysis (Al Sil G/UV plates, 90:10:5 CHCl<sub>3</sub>/ethanol/acetic acid). Plates were exposed for 24 h and analyzed with a Storm Phosphorimager. The identity of the YBT spot (*R<sub>F</sub>* = 0.39) was confirmed by atmospheric pressure chemical ionization mass spectrometry (YBT–iron complex ion<sup>4+</sup>: C<sub>21</sub>H<sub>24</sub>N<sub>3</sub>O<sub>4</sub>S<sub>3</sub>HFe<sup>+</sup>, *m/z* = 535.0) of samples purified by preparative TLC (data not shown). *M. tuberculosis* and *Y. pestis* were allowed to grow for approximately two generations before siderophore analysis. This growth takes place even in the presence of inhibitor owing to the residual iron, siderophore or both present in the relatively large inoculum used. Samples analyzed were corrected for small optical density differences observed between the inhibitor- and DMSO-treated cultures.

**Growth inhibition assays.** *M. tuberculosis* H37Rv was grown in GAST-D for iron-deficient conditions and in GAST-D supplemented with 200 μM FeCl<sub>3</sub> for iron-rich conditions. *Y. pestis* KIM6-2082.1+ was grown in PMH-D for iron-deficient conditions and in PMH-D supplemented with 200 μM FeCl<sub>3</sub> for iron-rich conditions. Salicyl-AMS was added (from a stock solution in DMSO) to the media at the concentrations indicated in **Figures 3d,e**. DMSO (0.5%) was added to the untreated controls. *M. tuberculosis* and *Y. pestis* cultures, inoculated at OD<sub>580</sub> = 0.01 and OD<sub>620</sub> = 0.005, respectively, were incubated in 96-well plates at 37 °C (200 μl/well; 8 d, stationary condition for *M. tuberculosis*; 22 h, 220 r.p.m. for *Y. pestis*) and growth was measured as optical density after incubation. IC<sub>50</sub> values were calculated by fitting the dose-response data (**Figs. 3d,e**) to the sigmoidal equation

$$\frac{OD_i}{OD_c} = b + \frac{(a - b)}{1 + ([I]/IC_{50})^s},$$

where OD<sub>i</sub> and OD<sub>c</sub> are optical densities of inhibitor-treated cultures and DMSO-treated controls, respectively, *a* and *b* are the top and bottom of the curve, respectively, and *s* is the slope (Hill coefficient). Data were fitted using Kaleidagraph software (Synergy Software).

**Accession codes.** BIND identifiers (<http://bind.ca/>): 262065, 262066, 262067.

*Note: Supplementary information is available on the Nature Chemical Biology website.*

#### ACKNOWLEDGMENTS

We dedicate this paper to Professor Christopher T. Walsh on the occasion of his 60<sup>th</sup> birthday. We thank R. Perry (University of Kentucky) for critical advice on *Y. pestis* experiments and G. Sukenick, A. Dudkina, H. Fang and S. Rusli (MSKCC Analytical Core Facility) and C. Soll (Hunter College/City University of New York MS Facility) for mass spectral analyses. D.S.T. acknowledges financial support from the William Randolph Hearst Fund in Experimental Therapeutics, William H. Goodwin and Alice Goodwin and the Commonwealth Foundation for Cancer Research, and the Experimental Therapeutics Center of MSKCC. L.E.N.Q., a Scholar of the Stavros S. Niarchos Foundation, acknowledges the financial

support of the Potts Memorial Foundation, the Cystic Fibrosis Association and the William Randolph Hearst Foundation.

#### COMPETING INTERESTS STATEMENT

The authors declare that they have no competing financial interests.

Received 15 March; accepted 15 April 2005

Published online at <http://www.nature.com/naturechemicalbiology/>

- Cole, S.T., Eisenach, K.D., McMurray, D.N. & Jacobs, W.R.J. (eds) *Tuberculosis and the Tubercle Bacillus* (ASM Press, Washington, DC, 2005).
- Perry, R.D. & Fetherston, J.D. *Yersinia pestis*—etiologic agent of plague. *Clin. Microbiol. Rev.* **10**, 35–66 (1997).
- Centers for Disease Control and Prevention. Biological and chemical terrorism: strategic plan for preparedness and response. Recommendations of the CDC strategic planning workgroup. *MMWR Recomm. Rep.* **49**, 1–14 (2000).
- Perry, R.D., Balbo, P.B., Jones, H.A., Fetherston, J.D. & DeMoll, E. Yersiniabactin from *Yersinia pestis*: biochemical characterization of the siderophore and its role in iron transport and regulation. *Microbiology* **145**, 1181–1190 (1999).
- Quadri, L.E.N. & Ratledge, C. Iron metabolism in the tubercle bacillus and other mycobacteria. In *Tuberculosis and the Tubercle Bacillus* (eds Cole, S.T., Eisenach, K.D., McMurray, D.N. & Jacobs, W.R.J.) 341–357 (ASM Press, Washington, DC, 2004).
- Bearden, S.W., Fetherston, J.D. & Perry, R.D. Genetic organization of the yersiniabactin biosynthetic region and construction of avirulent mutants in *Yersinia pestis*. *Infect. Immun.* **65**, 1659–1668 (1997).
- Gobin, J. & Horwitz, M.A. Exochelins of *Mycobacterium tuberculosis* remove iron from human iron-binding proteins and donate iron to mycobactins in the *M. tuberculosis* cell wall. *J. Exp. Med.* **183**, 1527–1532 (1996).
- De Voss, J.J. *et al.* The salicylate-derived mycobactin siderophores of *Mycobacterium tuberculosis* are essential for growth in macrophages. *Proc. Natl. Acad. Sci. USA* **97**, 1252–1257 (2000).
- Smith, I. Mycobacterium tuberculosis pathogenesis and molecular determinants of virulence. *Clin. Microbiol. Rev.* **16**, 463–496 (2003).
- Jurado, R.L. Iron, infections, and anemia of inflammation. *Clin. Infect. Dis.* **25**, 888–895 (1997).
- NIH-NIAID. The counter-bioterrorism research agenda of the National Institute of Allergy and Infectious Diseases (NIAID) for CDC category A agents (National Institutes of Health, Bethesda, Maryland, USA, 2002).
- Quadri, L.E.N. Assembly of aryl-capped siderophores by modular peptide synthetases and polyketide synthases. *Mol. Microbiol.* **37**, 1–12 (2000).
- Crosa, J.H. & Walsh, C.T. Genetics and assembly line enzymology of siderophore biosynthesis in bacteria. *Microbiol. Mol. Biol. Rev.* **66**, 223–249 (2002).
- Quadri, L.E.N., Sello, J., Keating, T.A., Weinreb, P.H. & Walsh, C.T. Identification of a *Mycobacterium tuberculosis* gene cluster encoding the biosynthetic enzymes for assembly of the virulence-conferring siderophore mycobactin. *Chem. Biol.* **5**, 631–645 (1998).
- Gehring, A.M., Mori, I.I., Perry, R.D. & Walsh, C.T. The nonribosomal peptide synthetase HMWP2 forms a thiazoline ring during biogenesis of yersiniabactin, an iron-chelating virulence factor of *Yersinia pestis*. *Biochemistry* **37**, 11637–11650 (1998).
- Kim, S., Lee, S.W., Choi, E.C. & Choi, S.Y. Aminoacyl-tRNA synthetases and their inhibitors as a novel family of antibiotics. *Appl. Microbiol. Biotechnol.* **61**, 278–288 (2003).
- Finking, R. *et al.* Aminoacyl adenylate substrate analogues for the inhibition of adenylate domains of nonribosomal peptide synthetases. *ChemBioChem* **4**, 903–906 (2003).
- Florini, J.R., Bird, H.H. & Bell, P.H. Inhibition of protein synthesis *in vitro* and *in vivo* by nucleocidin, an antitypanosomal antibiotic. *J. Biol. Chem.* **241**, 1091–1098 (1966).
- Quadri, L.E.N., Keating, T.A., Patel, H.M. & Walsh, C.T. Assembly of the *Pseudomonas aeruginosa* nonribosomal peptide siderophore pyochelin: *in vitro* reconstitution of aryl-4,2-bisthiazoline synthetase activity from PchD, PchE, and PchF. *Biochemistry* **38**, 14941–14954 (1999).
- May, J.J., Kessler, N., Marahiel, M.A. & Stubbs, M.T. Crystal structure of DhbE, an archetype for aryl acid activating domains of modular nonribosomal peptide synthetases. *Proc. Natl. Acad. Sci. USA* **99**, 12120–12125 (2002).
- Copeland, R.A. Tight binding inhibitors. In *Enzymes: A Practical Introduction to Structure, Mechanism, and Data Analysis* 305–317 (Wiley-VCH, New York, 2000).
- Zhu, X.-F., Williams, H.J. & Scott, A.I. Facile and highly selective 5'-desilylation of multi-silylated nucleosides. *J. Chem. Soc. Perkin Trans. I* 2305–2306 (2000).
- Castro-Pichel, J., Garcia-Lopez, M.T. & De las Heras, F.G. A facile synthesis of ascamycin and related analogs. *Tetrahedron* **43**, 383–389 (1987).
- Forrest, A.K. *et al.* Aminoalkyl adenylate and aminoacyl sulfamate intermediate analogues differing greatly in affinity for their cognate *Staphylococcus aureus* aminoacyl tRNA synthetases. *Bioorg. Med. Chem. Lett.* **10**, 1871–1874 (2000).
- Darwin, K.H., Ehrt, S., Gutierrez-Ramos, J.C., Weich, N. & Nathan, C.F. The proteasome of *Mycobacterium tuberculosis* is required for resistance to nitric oxide. *Science* **302**, 1963–1966 (2003).
- Barclay, R. & Ratledge, C. Mycobactins and exochelins of *Mycobacterium tuberculosis*, *M. bovis*, *M. africanum* and other related species. *J. Gen. Microbiol.* **134**, 771–776 (1988).
- Gong, S., Bearden, S.W., Geoffroy, V.A., Fetherston, J.D. & Perry, R.D. Characterization of the *Yersinia pestis* Yfu ABC inorganic iron transport system. *Infect. Immun.* **69**, 2829–2837 (2001).